Appendix 4

Remote sensing of ocean color: a methodology for dealing with broad spectral bands and significant out-of-band response

by

Howard R. Gordon

Department of Physics

University of Miami

Coral Gables, FL 33124

(Submitted for publication in *Applied Optics*)

Acknowledgment

The author wishes to thank K. Ding and F. He for helping with some of the computations, and the National Aeronautics and Space Administration for support under Grant NAGW-273 and Contracts NAS5-31363 and NAS5-31743.

Abstract

A methodology for delineating the influence of finite spectral band widths and significant out-of-band response of sensors for remote sensing of ocean color is developed and applied to the Sea-viewing Wide-Field-of-view Sensor (SeaWiFS). The basis of the method is the application of the sensor's spectral response functions to the individual components of the top-of-the-atmosphere (TOA) radiance rather than the TOA radiance itself. For engineering purposes, this approach allows one to assess easily (and quantitatively) the potential of a particular sensor design for meeting the system — sensor plus algorithms — performance requirements.

In the case of SeaWiFS, two significant conclusions are reached. First, it is found that the out-of-band effects on the water-leaving radiance component of the top of the atmosphere radiance are of the order of a few percent compared to a sensor with narrow spectral response. This implies that verification that the SeaWiFS system — sensor plus algorithms — meets the goal of providing the water-leaving radiance in the blue in clear ocean water to within 5% will require measurements of the water-leaving radiance over the entire visible spectrum as opposed to just narrow-band (10–20 nm) measurements in the blue. Second, it is it is found that the atmospheric correction of SeaWiFS can be degraded by the influence of water vapor absorption in the shoulders of the atmospheric correction bands in the near infrared. This absorption causes an apparent spectral variation of the aerosol component between these two bands that will be uncharacteristic of the actual aerosol present, leading to an error in correction. This effect is dependent on the water vapor content of the atmosphere. At typical water vapor concentrations the error is larger for aerosols with a weak spectral variation in reflectance than for those displaying a strong spectral variation. If the water vapor content is known, a simple procedure is provided to remove the degradation of the atmospheric correction. Uncertainty in the water vapor content will limit the accuracy of the SeaWiFS correction algorithm.

1. Introduction

In developing algorithms for ocean remote sensing data acquired by earth-orbiting satellites in the visible, where the spectrum of the radiance scattered by the ocean-atmosphere system in the atmospheric transmission windows is a relatively smooth function of wavelength, it is usually assumed that the spectral response of the instrument is a Dirac delta function, i.e., the necessary radiative transfer (RT) computations for a given spectral band are carried out at a single wavelength. In this paper a methodology is developed for adapting such computations to sensors with nominal spectral bandwidths $\sim$ 20–40 nm, and with significant out-of-band response. As a working example, we apply the analysis to the Sea-viewing Wide-Field-of-view Sensor (SeaWiFS)[1] scheduled for launch in 1995. The radiometric specifications of SeaWiFS are presented in the Appendix.

We begin by reviewing the decomposition of the measured atmosphere-leaving radiance into components resulting from Rayleigh scattering, aerosol scattering, and radiance backscattered out of the ocean. Then the process of combining the top of the atmosphere (TOA) radiance with the spectral response of the sensor is discussed and applied to the individual components of the TOA radiance using simulations that include the absorption of atmospheric Ozone but ignore the influence of other absorbing gases such as H_2O and O_2. The influence of absorption by these gases is then considered in the next section. Finally, the overall influence of the spectral band width and out-of-band response on atmospheric correction is discussed along with techniques for minimizing the effects in the case of SeaWiFS.

2. Decomposition of the measured radiance

Consider a spherical coordinate system at the sea surface with the z-axis toward the zenith and the x-y plane on the sea surface. A vector directed toward the sun has polar and azimuth angles θ_0 and ϕ_0, respectively, and a vector directed toward the sensor has polar and azimuth angles θ_v and ϕ_v, respectively. The radiance exiting the top of the atmosphere (TOA) in a direction specified by (θ_v, ϕ_v), $L_t(\lambda)$, at any wavelength λ is given by[2]

$$L_t(\lambda) = L_r(\lambda) + L_a(\lambda) + L_{ra}(\lambda) + tL_w(\lambda), \tag{1}$$

where L_r is the reflectance resulting from multiple scattering by air molecules (Rayleigh scattering) in the absence of aerosols, L_a is the reflectance resulting from multiple scattering by aerosols in the absence of the air, L_{ra} is the interaction term between molecular and aerosol scattering,[3] and L_w is the water-leaving reflectance. The term L_{ra} accounts for the interaction between Rayleigh and aerosol scattering, e.g., photons first scattered by the air then scattered by aerosols, or photons first scattered by aerosols then air, etc. This term is zero in the single scattering case, in which photons are only scattered once, and it can be ignored as long as the amount of multiple scattering is small, i.e., at small Rayleigh and aerosol optical thicknesses. The contribution from specular reflection of the solar beam from the sea surface (sun glitter) is ignored because the scan plane of most color sensors can be tilted to avoid the glitter pattern. In this equation, t is the diffuse transmittance of the atmosphere. It is approximated by

$$t(\theta_v, \lambda) = \exp\left[-\left(\frac{\tau_r(\lambda)}{2} + \tau_{Oz}(\lambda)\right)\left(\frac{1}{\mu_v}\right)\right] t_a(\theta_v, \lambda), \tag{2}$$

where

$$t_a(\theta_v, \lambda) = \exp\left[-\frac{[1 - \omega_a(\lambda)F_a(\mu_v, \lambda)]\tau_a(\lambda)}{\mu_v}\right], \tag{3}$$

$\mu_v = \cos\theta_v$, τ_r, τ_{Oz}, and τ_a are, respectively, the Rayleigh, Ozone, and aerosol optical thicknesses, and ω_a is the aerosol single scattering albedo. $F_a(\mu_v, \lambda)$ is related to the scattering phase function of the aerosol and is given by

$$F_a(\mu_v, \lambda) = \frac{1}{4\pi}\int_0^1 P_a(\alpha, \lambda)\, d\mu\, d\phi,$$

where $P_a(\alpha, \lambda)$ is the aerosol phase function at λ (normalized to 4π) for a scattering angle α, and

$$\cos\alpha = \mu\mu_v + \sqrt{(1 - \mu^2)(1 - \mu_v^2)}\cos\phi.$$

If θ_v is $\lesssim 60°$ the factor $[1 - \omega_a(\lambda)F_a(\mu_v, \lambda)]$ is usually $\ll 1$, so t_a depends only weakly on the aerosol optical thickness and is usually taken to be unity.

The retrieval of $L_w(\lambda)$ from $L_t(\lambda)$ is called atmospheric correction. To effect this, $L_r(\lambda) + L_a(\lambda) + L_{ra}(\lambda)$ must be estimated. The initial development of the atmospheric correction algorithm for the Coastal Zone Color Scanner[4,5] (CZCS), the proof-of-concept ocean color instrument, was based on the assumption of single scattering, wherein $L_{ra}(\lambda) = 0$ and

$$L_r(\lambda) = L_r^{ss}(\lambda) = F_0'(\lambda)\omega_r(\lambda)\tau_r(\lambda)p_r(\theta_v, \theta_0, \lambda)/4\pi\cos\theta_v. \tag{4}$$

where

$$p_r(\theta_v, \theta_0, \lambda) = P_r(\theta_-, \lambda) + \Big(r(\theta_v) + r(\theta_0)\Big) P_r(\theta_+, \lambda),$$

$$\cos\theta_\pm = \pm \cos\theta_0 \cos\theta_v - \sin\theta_0 \sin\theta_v \cos(\phi_v - \phi_0),$$

$\omega_r = 1$, P_r is the Rayleigh scattering phase function, and $r(\alpha)$ is the Fresnel reflectance of the air-sea interface for an incident angle α. $F_0'(\lambda)$ is the instantaneous extraterrestrial solar irradiance $F_0(\lambda)$ reduced by two trips through the Ozone layer, i.e.,

$$F_0'(\lambda) = F_0(\lambda) T_{Oz}(\lambda) = F_0(\lambda) \exp\Big[-\tau_{Oz}(\lambda) M\Big] \tag{5}$$

where $T_{Oz}(\lambda)$ is the two-way transmittance of the Ozone layer, $\tau_{Oz}(\lambda)$ is the Ozone optical thickness, and M is the two-way air mass:

$$M = \left(\frac{1}{\cos\theta_v} + \frac{1}{\cos\theta_0}\right).$$

The aerosol radiance in the single scattering approximation, $L_a^{ss}(\lambda)$, is given by a similar expression with the subscript "r" replaced by "a" for aerosol ($\omega_a \leq 1$). Typically the single scattering approximation leads to an error of $\lesssim 5\%$ in $L_r(\lambda)$.[6] In contrast, the error in $L_a + L_{ra}$ estimated by single scattering is of the order of 30–90%, depending on the aerosol model and geometry;[2] however, $L_a + L_{ra}$ is approximately $\propto L_a^{ss}$, i.e.,

$$L_a(\lambda) + L_{ra}(\lambda) = C(\theta_v, \phi_v, \theta_0, \phi_0, L_a^{ss}(\lambda), \lambda)\, L_a^{ss}(\lambda), \tag{6}$$

where $C(\theta_v, \phi_v, \theta_0, \phi_0, L_a^{ss}(\lambda), \lambda)$ depends only weakly on $L_a^{ss}(\lambda)$ and λ. For example, for the simulations presented in Figures 1 and 2 of Ref. 2 for $\theta_0 = 60°$, $\phi_0 = 0$, $\theta_v \approx 45°$, and $\phi_v = 90°$, the quantity $C(\theta_v, \phi_v, \theta_0, \phi_0, L_a^{ss}(\lambda), \lambda)$ shows a near-linear dependence on $L_a^{ss}(\lambda)$, and varies from ~ 1.79 at 865 nm to ~ 1.88 at 443 nm for the Maritime aerosol model with a relative humidity of 98% (M98), while for the Tropospheric model with a relative humidity of 70% (T70), the corresponding variation was from ~ 1.33 to ~ 1.26. In contrast, the values of $L_a^{ss}(443)/L_a^{ss}(865)$ ranged from 1.9 for M98 to 4.2 for T70. Thus, the spectral variation of $L_a^{ss}(\lambda)$ far exceeds that of $C(\theta_v, \phi_v, \theta_0, \phi_0, L_a^{ss}(\lambda), \lambda)$. Note, however, that the spectral variation in $L_a^{ss}(\lambda)$ is still small compared to $L_r^{ss}(\lambda)$: $L_r^{ss}(443)/L_r^{ss}(865) \approx 28$.

In the proposed SeaWiFS atmospheric correction algorithm,[2] all of the effects of multiple scattering are included, e.g., L_r is computed using a multiple scattering code (including polarization).

However, for the purposes of including the effects of the sensor's spectral response, it is legitimate to utilize the single scattering approximation, i.e., $L_r(\lambda) = L_r^{ss}(\lambda)$ and

$$L_a(\lambda) + L_{ra}(\lambda) = C(\theta_v, \phi_v, \theta_0, \phi_0) L_a^{ss}(\lambda), \tag{7}$$

since the L_r^{ss} and L_a^{ss} terms contain nearly all of the *spectral* variation of L_r and $L_a + L_{ra}$, respectively. Note, we will now assume an $L_a^{ss}(\lambda)$- and wavelength-independent $C(\theta_v, \phi_v, \theta_0, \phi_0, L_a^{ss}(\lambda), \lambda)$, i.e., the aerosol *multiple* scattering effects are assumed to be independent of $L_a^{ss}(\lambda)$ and wavelength.

3. Band averaging

We now compute the expected radiance at the sensor, given the spectral response $S_i(\lambda)$ of the i^{th} spectral band. $S_i(\lambda)$ provides the output current (or voltage) from the detector for a unit radiance of wavelength λ, e.g., $\int S_i(\lambda)\, d\lambda$ would be the output current for a *spectrally flat* source of radiance of magnitude 1 mW/cm^2μm Sr. We define the "band" radiance for the i^{th} spectral band when viewing a source of radiance $L(\lambda)$ to be

$$\langle L(\lambda) \rangle_{S_i} \equiv \frac{\int L(\lambda) S_i(\lambda)\, d\lambda}{\int S_i(\lambda)\, d\lambda} \tag{8}$$

The output current (or voltage) will then be $\propto \langle L(\lambda) \rangle_{S_i}$.

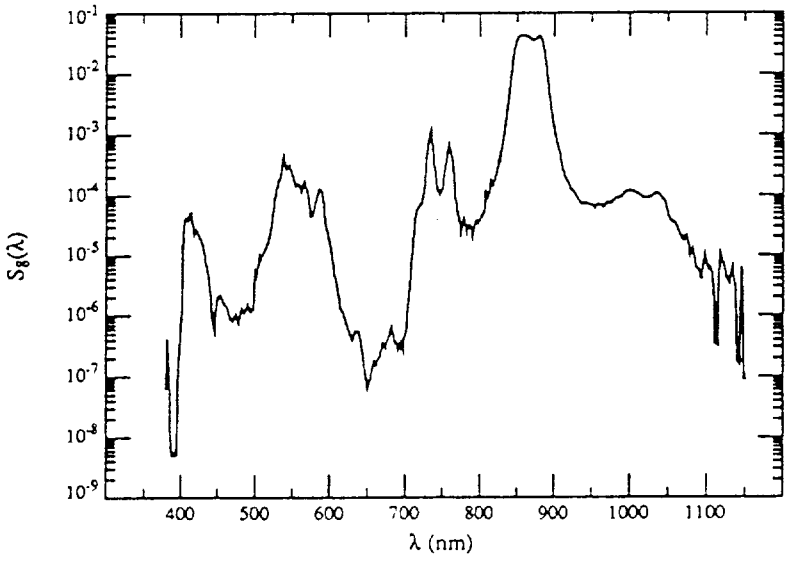

Figure 1. Spectral response of SeaWiFS band 8, normalized such that $\int S_8(\lambda)\, d\lambda = 1$. Data are taken from Barnes et al.[7]

In the case of SeaWiFS, some bands have significant out-of-band response. An example is shown in Figure 1 which provides S_8 for Band 8, nominally 845–885 nm. Note the significant response from $\sim$ 520–580 nm and near 750 nm. In fact, when viewing a source for which $L(\lambda) \propto \lambda^{-4} F_0(\lambda)$, e.g., L_r^{**}, approximately 9% of the signal in Band 8 derives from $\lambda < 600$ nm. In contrast, only about 0.7% of the signal derives from $\lambda < 600$ nm for a spectrally flat source.

3.A. Band-averaged L_r

In the notation of Eq. (8),

$$\langle L_r(\lambda)\rangle_{S_i} = \langle \tau_r(\lambda) F_0'(\lambda)\rangle_{S_i} G(\theta_0, \theta_v, \phi_v),$$

where $G(\theta_0, \theta_v, \phi_v)$ is a purely geometrical factor. If we ignored the presence of the Ozone layer, $F_0' = F_0$, and we could write

$$\langle \tau_r(\lambda) F_0(\lambda)\rangle_{S_i} = \langle \tau_r(\lambda)\rangle_{F_0 S_i} \langle F_0(\lambda)\rangle_{S_i},$$

where

$$\langle \tau_r(\lambda)\rangle_{F_0 S_i} \equiv \frac{\int \tau_r(\lambda) F_0(\lambda) S_i(\lambda)\, d\lambda}{\int F_0(\lambda) S_i(\lambda)\, d\lambda}. \tag{9}$$

This is very convenient because it separates τ_r and F_0 and allows us to carry out the computation of $I_r \equiv L_r / F_0$ for Band i by using $\langle \tau_r(\lambda)\rangle_{F_0 S_i}$ for the Rayleigh optical thickness. Multiplication of I_r by $\langle F_0(\lambda)\rangle_{S_i}$ then yields the desired $\langle L_r(\lambda)\rangle_{S_i}$. To include the effect of Ozone, we hypothesize that since $\tau_{Oz} M \ll 1$,

$$\langle \tau_r(\lambda) F_0'(\lambda)\rangle_{S_i} \approx \langle \tau_r(\lambda)\rangle_{F_0 S_i} \langle F_0(\lambda)\rangle_{S_i} \exp\left[-\langle \tau_{Oz}(\lambda)\rangle_{F_0 S_i} M\right]. \tag{10}$$

We tested this hypothesis by utilizing the predicted $S_i(\lambda)$ for the SeaWiFS bands.[7] To effect the test, $\tau_r(\lambda)$ was taken from Travis and Hansen:[8]

$$\tau_r = 0.008569\lambda^{-4}\left(1 + 0.0113\lambda^{-2} + 0.00013\lambda^{-4}\right), \tag{11}$$

where λ is in μm. Following André and Morel[9] the Ozone absorption coefficient $k_{Oz}(\lambda)$ was taken from Nicolet.[10] The value of τ_{Oz} is related to k_{Oz} by

$$\tau_{Oz}(\lambda) = k_{Oz}(\lambda)\frac{DU}{1000},$$

where DU is the Ozone concentration in mAtm-cm (Dobson Units). $F_0(\lambda)$ was taken from Neckel and Labs.[11] Table 1 provides a comparison between the right- and left-hand sides of Eq. (10) for an Ozone concentration of 350 DU. The large % difference for Band 8 is due to the significant out-

Table 1: % difference between the right (R) and left (L) sides of Eq. (10) for $M = 3$ for the SeaWiFS bands.

Band	100%(L-R)/L
1	−0.008
2	−0.010
3	−0.055
4	+0.106
5	−0.168
6	−0.010
7	−0.031
8	−0.499

of-band response between 500 and 600 nm; however, for $\theta_0 = 60°$ and nadir viewing ($M = 3$), this error translates to an error in $\langle L_r(\lambda)\rangle_{S_i}$ of $\sim 1/3$ to $2/3$ the quantization increment of the SeaWiFS on-board 10-bit digitizer (depending on the amplifier gain setting), i.e., less than 1 digital count

Table 2: Quantities needed to compute $\langle L_r(\lambda)\rangle_{S_i}$ and $L_r(\lambda_i)$ for the SeaWiFS bands.

Band (i)	$\langle \tau_r(\lambda)\rangle_{F_0 S_i}$	$\tau_r(\lambda_i)$	$\langle F_0(\lambda)\rangle_{S_i}$ mW/cm^2 μm sr	$F_0(\lambda_i)$ mW/cm^2 μm sr	$\langle k_{Oz}(\lambda)\rangle_{F_0 S_i}$ (×1000)	$k_{Oz}(\lambda_i)$ (×1000)
1	0.3132	0.3185	170.79	180.80	1.03	0.81
2	0.2336	0.2361	189.45	194.95	4.00	3.75
3	0.1547	0.1560	193.66	198.85	25.36	22.27
4	0.1330	0.1324	188.35	193.65	42.00	42.50
5	0.0947	0.0938	185.33	190.25	93.38	90.38
6	0.0446	0.0436	153.41	153.50	46.85	45.92
7	0.0256	0.0255	122.24	122.40	8.37	7.42
8	0.0169	0.0155	98.82	97.10	4.85	3.71

(DC) from the sensor. Thus, we will employ the approximation in Eq. (10) to treat the influence of Ozone absorption on all three terms in Eq. (1). Specifically, whenever τ_{Oz} occurs, the spectral averages will be computed assuming $\tau_{Oz} = 0$, and τ_{Oz} will be reintroduced into the final result

by replacing it with $\langle \tau_{Oz}(\lambda) \rangle_{F_0 S_i}$. The fact that the approximation is sufficiently accurate for computing $\langle L_r(\lambda) \rangle_{S_i}$ insures that it will be for the terms in Eq. (1) with weaker spectral variation, e.g., $L_a(\lambda)$. The values of $\langle \tau_r(\lambda) \rangle_{F_0 S_i}$, $\langle F_0(\lambda) \rangle_{S_i}$, and $\langle k_{Oz}(\lambda) \rangle_{F_0 S_i}$ for the SeaWiFS bands are provided in Table 2. Note that the ($\times$1000) notation for $\langle k_{Oz}(\lambda) \rangle_{F_0 S_i}$ means that the entries in the table have been multiplied by 1000, i.e., $\langle k_{Oz}(\lambda) \rangle_{F_0 S_i} = 1.03 \times 10^{-3}$ for Band 1. Table 2 also provides $\tau_r(\lambda_i)$, $F_0(\lambda_i)$, and $k_{Oz}(\lambda_i)$, where henceforth λ_i with $i = 1$ to 8 refers to the nominal wavelength of the band center of SeaWiFS Band i.

To assess the efficacy of the above techniques for determining $\langle L_r(\lambda) \rangle_{S_i}$ in the multiple scattering regime, we have computed multiple scattering values for this quantity for $\theta_0 = 60°$ and nadir viewing in two ways. First, $I_r(\lambda)$ was computed as a function of λ using $\tau_r(\lambda)$ and a multiple scattering (scalar) RT code. From this,

$$L_r(\lambda) = I_r(\lambda) F_0(\lambda) \exp[-\tau_{Oz}(\lambda) M]$$

was formed and the average, $\langle L_r(\lambda) \rangle_{S_i}$, over the SeaWiFS bands was computed directly. To effect this for fine increments in λ, $I_r(\lambda)$ was linearly interpolated from log-transformed values of $I_r(\lambda_i)$ and λ_i computed at 10 wavelengths, the nominal SeaWiFS band centers plus 380 and 1150 nm. This average is taken as the "correct" answer for the average. Second, the same RT code was

Table 3: % difference between the estimated (E) and correct (C) values of $\langle L_r(\lambda) \rangle_{S_i}$ as described in the text.

Band	100%(E-C)/C
1	+0.15
2	+0.12
3	+0.02
4	−0.01
5	−0.09
6	−0.01
7	−0.09
8	−0.05

operated with $\tau_r(\lambda_i)$ replaced by $\langle \tau_r(\lambda) \rangle_{F_0 S_i}$ to compute I_r for the i^{th} band, $I_r(i)$. Then, $\langle L_r(\lambda) \rangle_{S_i}$ was estimated from

$$\langle L_r(\lambda) \rangle_{S_i} = I_r(i) \langle F_0(\lambda) \rangle_{S_i} \exp[-\langle \tau_{Oz}(\lambda) \rangle_{F_0 S_i} M]. \quad (12)$$

This is similar to the method employing single scattering with $I_r(i)$ replacing $\langle \tau_r(\lambda) \rangle_{F_0 S_i} G(\theta_0, \theta_v, \phi_v)$. The resulting $\langle L_r(\lambda) \rangle_{S_i}$ is the "estimated" band-averaged $L_r(\lambda)$. Table 3 provides the % difference between the estimated and correct values of $\langle L_r(\lambda) \rangle_{S_i}$, for $\theta_0 = 60°$, nadir viewing, and an Ozone concentration of 350 DU. It is clear that Eq. (12) is capable of estimating the radiance to very high accuracy. In fact, in this example, the error is less than 1 DC for all of the SeaWiFS bands. Also, the excellent performance of the estimator attests to the viability of the treatment of the Ozone absorption.

3.B. Band-averaged $L_a + L_{ra}$

From Eq. (7), we see that the band-averaged aerosol component can be found by considering $L_a^{ss}(\lambda)$. At the core of both the CZCS and SeaWiFS atmospheric correction algorithms is the spectral variation of the normalized single-scattered aerosol radiance, i.e., $I_a^{ss}(\lambda) \equiv L_a^{ss}(\lambda)/F_0(\lambda)$. Two single wavelengths λ and λ_0 are used to define the atmospheric correction parameters $\varepsilon(\lambda, \lambda_0)$ given by

$$\varepsilon(\lambda, \lambda_0) = \frac{I_a^{ss}(\lambda)}{I_a^{ss}(\lambda_0)}. \tag{13}$$

Thus,

$$L_a^{ss}(\lambda) = F_0(\lambda) \varepsilon(\lambda, \lambda_0) I_a^{ss}(\lambda_0), \tag{14}$$

and

$$\langle L_a^{ss}(\lambda) \rangle_{S_i} = \langle F_0(\lambda) \rangle_{S_i} \langle \varepsilon(\lambda, \lambda_0) \rangle_{F_0 S_i} I_a^{ss}(\lambda_0). \tag{15}$$

Note that λ_0 is an arbitrary (single) wavelength; here we take it to be to be 865 nm, the nominal band center of SeaWiFS Band 8. Also, we have set $\tau_{Oz} = 0$. Ozone can be included as stated earlier by replacing $\langle F_0(\lambda) \rangle_{S_i}$ by $\langle F_0(\lambda) \rangle_{S_i} \exp[-\langle \tau_{Oz}(\lambda) \rangle_{F_0 S_i} M]$ in the final result. To proceed further, we need $\varepsilon(\lambda, \lambda_0)$, which can be computed using Eq. (4) with the subscript "r" replaced by "a" for aerosol. Wang and Gordon[12] have shown that for the aerosol models proposed by Shettle and Fenn[13] for LOWTRAN-6,[14] and used in Ref. 2, $\varepsilon(\lambda, \lambda_0)$ can be approximated by

$$\varepsilon(\lambda, \lambda_0) \approx \exp[c(\lambda_0 - \lambda)] \tag{16}$$

with $\lambda < \lambda_0$. The limits on c over the range 412 to 865 nm for the models that they[12] used were $0 \lesssim c \lesssim 1.9 \times 10^{-3}$ nm^{-1}. This equation is sufficiently accurate to examine the out-of-band effects on the aerosol component. Table 4 provides $\langle \varepsilon(\lambda, 865) \rangle_{F_0 S_i}$ and $\varepsilon(\lambda_i, 865)$, where λ_i is the

nominal center wavelength of Band i, and their % difference for $c = 2 \times 10^{-3}$ nm^{-1}. We note that,

Table 4: $\langle \varepsilon(\lambda, 865) \rangle_{F_0 S_i}$, $\varepsilon(\lambda_i, 865)$, and their % difference for $c = 2 \times 10^{-3}$ nm^{-1}.

Band	$\langle \varepsilon(\lambda, 865) \rangle_{F_0 S_i}$	$\varepsilon(\lambda_i, 865)$	% Diff.
1	2.4645	2.4744	−0.40
2	2.3192	2.3257	−0.28
3	2.1113	2.1170	−0.27
4	2.0350	2.0340	+0.05
5	1.8584	1.8590	+0.03
6	1.4842	1.4770	+0.49
7	1.2202	1.2214	−0.10
8	1.0131	1.0000	+1.31

with the exception of Band 8, the effect of the out-of-band response is $\lesssim 0.5\%$ of the nominal $\varepsilon(\lambda_i, 865)$. Thus, with the exception of Band 8, $\langle \varepsilon(\lambda, 865) \rangle_{F_0 S_i}$ should follow Eq. (16) nearly as well as $\varepsilon(\lambda_i, 865)$, i.e., the spectral variations of $\langle \varepsilon(\lambda, 865) \rangle_{F_0 S_i}$, $i = 1$ to 7, and $\varepsilon(\lambda_i, 865)$ will be nearly identical. This conclusion will be modified by the presence of gaseous absorption (Section 4B).

3.C. Band-averaged tL_w

The water-leaving radiance varies strongly with the pigment concentration, C, defined to be the sum of the concentrations of chlorophyll a and phaeophytin a. For band averaging purposes, we use the model proposed by Gordon et al.[15] This model yields the normalized water-leaving radiance, $[L_w(\lambda)]_N$ defined according to[16]

$$L_w(\lambda) = t(\theta_0, \lambda) \cos\theta_0 \, [L_w(\lambda)]_N,$$

as a function of C. It agrees well with the measurements of Clark[17] for $\lambda \lesssim 600$ nm. Disagreement in the red is thought to be due to the effects of instrument self shading.[18] It is convenient here to switch from radiance L to reflectance ρ defined to be $\pi L / F_0 \cos\theta_0$. The normalized water-leaving reflectance is then

$$[\rho_w(\lambda)]_N = \frac{\pi [L_w(\lambda)]_N}{F_0(\lambda)}.$$

Combining these two equations yields the desired

$$t(\theta_v, \lambda) L_w(\lambda) = \frac{\cos\theta_0}{\pi} t(\theta_v, \lambda) t(\theta_0, \lambda) F_0(\lambda) [\rho_w(\lambda)]_N,$$

and to assess band averaging, we need to compute $\langle t(\theta_v, \lambda) L_w(\lambda) \rangle_{S_i}$. We have carried out this computation for two pigment concentrations, $C = 0.03$ and 1.0 mg/m^3. The $[\rho_w(\lambda)]_N$ spectra used in the computation are provided in Figure 2. The reflectances presented for $\lambda > 700$ nm

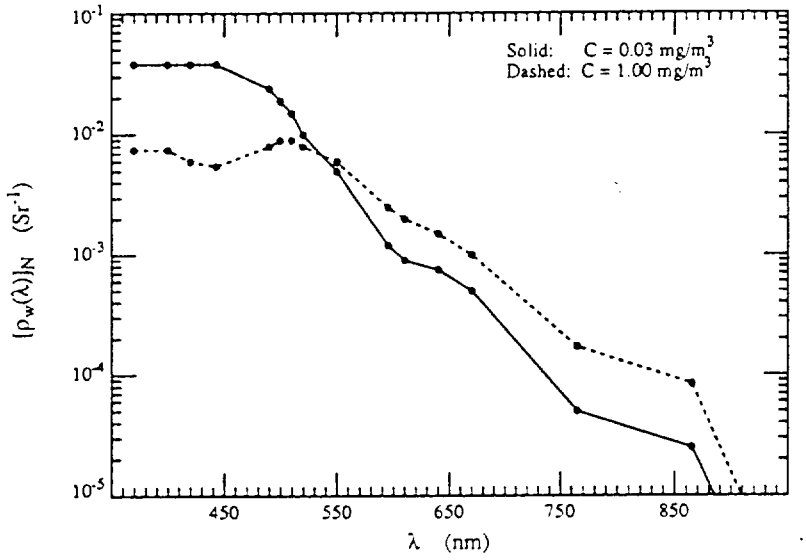

Figure 2. $[\rho_w(\lambda)]_N$ for $C = 0.03$ and 1.0 mg/m^3. Model computations were carried out at the points indicated by dots and interpolated to other wavelengths.

are estimated based on the absorption coefficient of water and the expected backscattering of phytoplankton. Measurements of L_w or the ocean backscattering properties have never been carried out at these wavelengths. Noting that $[\rho_w(\lambda)]_N$ varies by three orders of magnitude over the spectral range of interest (compared to a factor of ~ 33 for L_r), we expect that the out-of-band effects on tL_w for the red and NIR bands will be very severe. To calculate the required integrals, log-linear interpolation was used to estimate $[\rho_w(\lambda)]_N$, i.e., straight lines connecting the points on Figure 2. The reflectance was arbitrarily taken to be 10^{-10} Sr^{-1} at $\lambda = 1150$ nm. The band averaging yields

$$\langle t(\theta_v, \lambda) L_w(\lambda) \rangle_{S_i} = \frac{\cos\theta_0}{\pi} \langle F_0(\lambda) \rangle_{S_i} \langle t(\theta_v, \lambda) t(\theta_0, \lambda) [\rho_w(\lambda)]_N \rangle_{F_0 S_i}$$

We computed $\langle t(\theta_v,\lambda)t(\theta_0,\lambda)[\rho_w(\lambda)]_N\rangle_{F_0S_i}$ for C = 0.03 and 1.0 mg/m^3, and M = 2. The value M = 2, its minimum, was chosen to provide the strongest variation of tL_w with λ. This average is compared with $t(\theta_v,\lambda_i)t(\theta_0,\lambda_i)[\rho_w(\lambda_i)]_N$ in Table 5. The differences between X_i and Y_i are

Table 5: Comparison between the quantities
$X_i \equiv \langle t(\theta_v,\lambda)t(\theta_0,\lambda)[\rho_w(\lambda)]_N\rangle_{F_0S_i}$
and $Y_i \equiv t(\theta_v,\lambda_i)t(\theta_0,\lambda_i)[\rho_w(\lambda_i)]_N$ for
C = 0.03 and 1.0 mg/m^3, and M = 2.
The notation "2.77−2" etc., stands for 2.77×10^{-2}.

Band	C = 0.03 mg/m^3				C = 1.0 mg/m^3			
i	X_i	Y_i	% Diff.	DC Diff.	X_i	Y_i	% Diff.	DC Diff.
1	2.77−2	2.76−2	+3.6−1	+0.4	4.73−3	4.77−3	−8.7−1	−0.13
2	2.90−2	2.99−2	−3.2−0	−4.4	4.54−3	4.34−3	+4.6−0	+0.82
3	1.91−2	2.02−2	−5.4−0	−6.7	6.86−3	6.74−3	+1.7−0	+0.72
4	1.25−2	1.28−2	−1.7−0	−1.5	7.36−3	7.65−3	−3.8−0	−2.00
5	3.87−3	3.65−3	+6.1−0	+1.8	4.61−3	4.65−3	−1.0−0	−0.39
6	7.65−4	4.64−4	+6.5+1	+3.6	9.60−4	9.28−4	+3.4−0	+0.37
7	7.15−5	4.84−5	+4.7+1	+0.3	1.81−4	1.65−4	+1.0+1	+0.22
8	1.03−4	2.45−5	+3.2+2	+1.2	1.34−4	8.25−5	+6.3+1	+0.76

explained by the spectral shapes of $S_i(\lambda)$ and $L_w(\lambda)$. If S_i has a weak out-of-band maximum to the long-wave side of the band center maximum, X_i will be $< Y_i$ if $L_w(\lambda)$ decreases strongly with increasing wavelength, and vice versa if $L_w(\lambda)$ increases with λ. Bands 2 and 3 are examples of this behavior, for which a shift in the sign of $X_i - Y_i$ occurs between C = 0.03 and 1.0 mg/m^3. In contrast, Band 4 has secondary maxima on both sides of the band center (at $\sim$ 440 nm and 600 nm) and $X_i < Y_i$ at both concentrations. As expected, the long-wave bands show significant differences between X_i and Y_i with $X_i > Y_i$ due to light leakage from the blue and green (Figure 1). However, the difference is $\lesssim$ 1 DC in the NIR atmospheric correction bands, and it would appear that it is reasonable to assume that X_i = 0 in these bands. Noting that the goal of SeaWiFS is to retrieve $\langle L_w(\lambda)\rangle_{S_i}$ in Band 2 in clear water ($C \approx 0.03$ mg/m^3) with an error of $\leq 5\%$, Table 5 underscores the importance of measuring, or at least estimating, the full spectrum of L_w for the validation of satellite-retrieved $\langle L_w(\lambda)\rangle_{S_i}$.

In the spirit of our method for dealing with Ozone absorption, i.e., Eq. (10), we have tried to approximate $\langle t(\theta_v,\lambda)t(\theta_0,\lambda)[\rho_w(\lambda)]_N\rangle_{F_0S_i}$ by

$$\langle t(\theta_v,\lambda)t(\theta_0,\lambda)[\rho_w(\lambda)]_N\rangle_{F_0S_i} \approx t(\theta_v,i)t(\theta_0,i)\langle[\rho_w(\lambda)]_N\rangle_{F_0S_i}, \tag{17}$$

where

$$t(\theta,i) = \exp\left[-\left(\frac{\langle\tau_r(\lambda)\rangle_{F_0S_i}}{2} + \langle\tau_{Oz}(\lambda)\rangle_{F_0S_i}\right)\frac{1}{\cos\theta}\right]. \tag{18}$$

The % difference between the left- and right-hand-sides of Eq. (17) for $C = 0.03$ mg/m^3 and $M = 3$ is provided in Table 6. Clearly, the approximation is sufficiently accurate to estimate

Table 6: % difference between the right (R) and left (L) sides of Eq. (17) for $M = 3$ for the SeaWiFS bands.

Band	100%(R-L)/R
1	− 0.01
2	+ 0.01
3	+ 0.11
4	+ 0.18
5	+ 0.76
6	+ 2.62
7	+ 7.48
8	+25.28

$\langle t(\theta_v,\lambda)L_w(\lambda)\rangle_{S_i}$ in the visible bands.

4. Gas Absorption

With the exception of Ozone, to this point we have ignored the absorption of atmospheric gases, i.e., H_2O and O_2. In the case of SeaWiFS, only Band 7 (745–785 nm) was forced to encompass a gas absorption band, the O_2 A band ($\sim 759 - 770$ nm), to provide an adequate signal-to-noise ratio. The other SeaWiFS bands have been placed in absorption-free atmospheric windows. However, even for spectral bands in the atmospheric windows, the effect of absorption may be important in the case of significant out-of-band response. For example, Figure 3 provides the spectral response of SeaWiFS Band 8 along with the H_2O-O_2 surface-to-zenith atmospheric transmittance (on a linear scale) from LOWTRAN.[14,19] Clearly, the H_2O absorption near 730, 850, and 890 nm, and the O_2

absorption near 760 nm will have some influence on the radiance measured in this spectral band. Also, the absence of gas absorption features for $\lambda \lesssim 570$ nm suggests that, other than Ozone, gas absorption below this wavelength can be ignored.

4.A. Influence on L_r

Within the framework we have developed for band averaging, the correct way of accurately including gas absorption would be to carry out detailed line-by-line radiative transfer computations through the absorption bands, e.g., in the case of the Rayleigh scattering component the "correct" value of $\langle L_r(\lambda)\rangle_{S_i}$ in Table 3 should be computed using an RT program that includes line-by-line, or at least narrow-band, absorption such as LOWTRAN. Unfortunately, LOWTRAN provides only

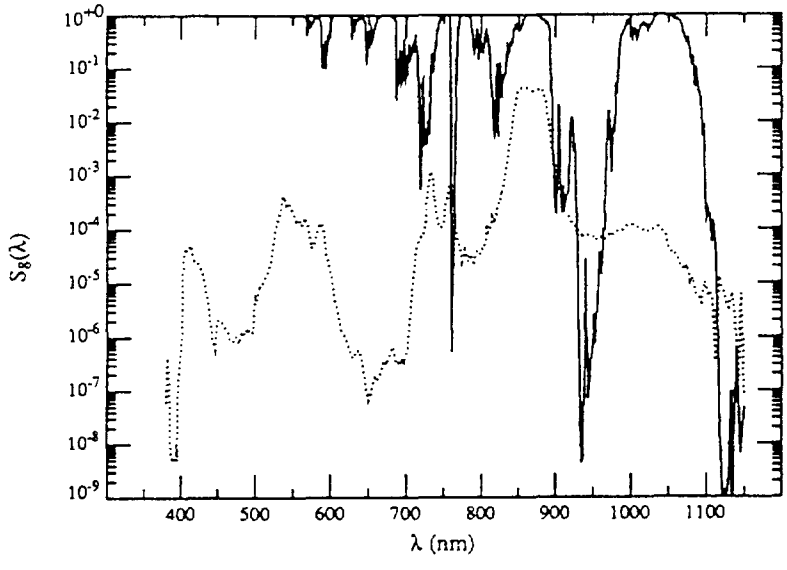

Figure 3. SeaWiFS Band 8 spectral response (dotted line) and atmospheric transmittance of H_2O and O_2 (solid line) for the LOWTRAN Tropical atmosphere (most water vapor). H_2O and O_2 transmittance is on a linear scale such that $10^{-1} \Rightarrow$ a transmittance of 0.9, $10^{-2} \Rightarrow$ a transmittance of 0.8, etc.

an approximate treatment of multiple scattering, and has no provision for a specularly reflecting lower boundary. However, since we expect the effect of gas absorption arising from the out-of band response to be small, highly accurate radiances are not really required for assessing the influence of

gas absorption. Thus, we will try to make a first-order estimate using LOWTRAN. To effect this, we computed $I_r = L_r/F_0$ for an aerosol-free atmosphere with a totally absorbing lower boundary (albedo = 0) for $\theta_0 = 60°$ and $\theta_v = 0$ ($M = 3$) using LOWTRAN. Ozone was removed under the assumption that it resides in a nonscattering layer at the TOA with the concentration that was used in the LOWTRAN calculations. This provided $I_r^{abs}(\lambda)$, the normalized Rayleigh component in the presence of absorption. Our multiple scattering code was then used in the same configuration to provide I_r at a select number of wavelengths (SeaWiFS band centers along with 380 and 1150 nm). These were interpolated as described in Section 3A to provide $N_r(\lambda)$, the normalized Rayleigh component in the absence of absorption. If LOWTRAN treated multiple scattering properly, $N_r(\lambda)$ and $I_r^{abs}(\lambda)$ would be identical in the atmospheric windows. This was forced by multiplying $I_r^{abs}(\lambda)$ by

$$1.015\, T_{O_3}^{-1}\left[1 - a(1050 - \lambda)^2\right]^{-1},$$

where $a = 1.5 \times 10^{-7}$ nm^{-2} and λ is in nm, to yield $A_r(\lambda)$, the Rayleigh component in the presence of absorption, and including a corrected treatment of multiple scattering. Thus, the principal difference between $N_r(\lambda)$ and $A_r(\lambda)$ is the absorption bands. Figure 4 provides this difference (%) showing the influence of the absorption bands for the LOWTRAN Subarctic winter atmosphere (the

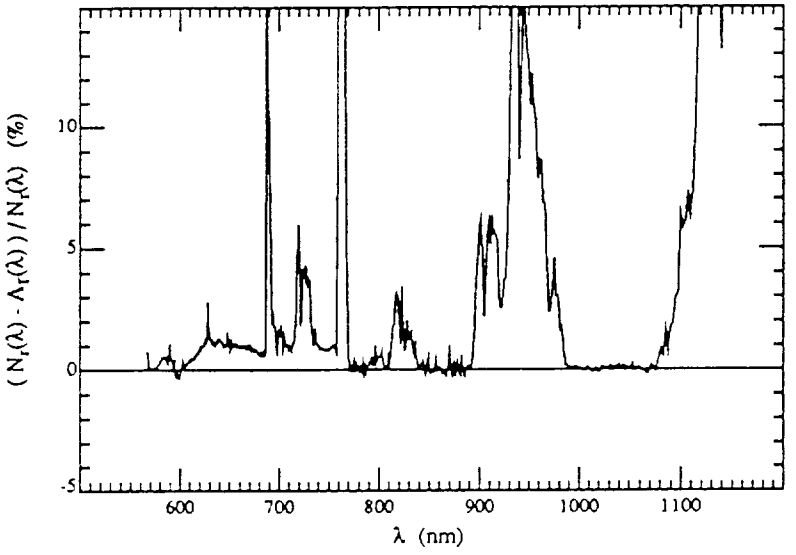

Figure 4. Difference between $N_r(\lambda)$ and $A_r(\lambda)$ as a function of λ for the LOWTRAN Subarctic winter atmosphere (least water vapor) and $M = 3$ as described in the text.

smallest LOWTRAN water vapor concentration). The influence of the gas absorption bands on the band-averaged radiances is provided by the difference between $\langle N_r(\lambda)F_0(\lambda)\rangle_{S_i}$ and $\langle A_r(\lambda)F_0(\lambda)\rangle_{S_i}$. This is presented in Table 7 as a % difference and a DC difference for Bands 6–8. For Bands 1–5, this difference is $\lesssim 0.02$ DC because the principal out-of-band maxima for these are in the blue and green. In the preparation of Table 7, the O_2 A absorption band has been removed from the Band 7 computation of $\langle A_r(\lambda)F_0(\lambda)\rangle_{S_i}$, since Ding and Gordon[20] have provided a method of accounting for this in-band absorption feature. However, it has been included in the computations for all other bands. We note that with the exception of Band 6, the error in using $\langle N_r(\lambda)F_0(\lambda)\rangle_{S_i}$,

Table 7: $\langle N_r(\lambda)F_0(\lambda)\rangle_{S_i} - \langle A_r(\lambda)F_0(\lambda)\rangle_{S_i}$ in % and in DC (in parenthesis) for $\theta_0 = 60°$ and nadir viewing.

LOWTRAN model	H_2O g/cm^2	Band 6	Band 7	Band 8
Tropical	3.322	1.23 (1.58)	0.64 (0.52)	0.82 (0.50)
Midlatitude summer	2.356	0.86 (1.10)	0.47 (0.38)	0.55 (0.34)
Midlatitude winter	0.686	0.86 (1.10)	0.39 (0.32)	0.46 (0.28)
Subarctic summer	1.653	1.20 (1.53)	0.69 (0.56)	0.84 (0.51)
Subarctic winter	0.328	0.94 (1.20)	0.39 (0.32)	0.28 (0.17)
U.S. Standard	1.125	1.07 (1.37)	0.51 (0.42)	0.58 (0.35)

i.e., in ignoring gas absorption, is usually $\lesssim 0.5$ DC and is therefore undetectable with SeaWiFS. In Band 6 the error is usually ~ 1 DC, but can reach ~ 1.5 DC. This is principally due to the O_2 B absorption band which overlaps the long-wave shoulder of Band 6 (O_2 B band head is at ~ 686 nm). Similar computations have been carried out for $\theta_0 = 0$ and 40°. These results of these for the U.S Standard atmosphere are presented in Table 8. These results suggest that the error imposed

Table 8: $\langle N_r(\lambda)F_0(\lambda)\rangle_{S_i} - \langle A_r(\lambda)F_0(\lambda)\rangle_{S_i}$ in % and in DC (in parenthesis) for the U.S. Standard atmosphere with nadir viewing.

θ_0	Band 6	Band 7	Band 8
0°	0.61 (1.22)	0.29 (0.38)	0.35 (0.34)
40°	0.61 (0.99)	0.27 (0.28)	0.28 (0.21)
60°	1.07 (1.37)	0.51 (0.42)	0.58 (0.35)

by ignoring the gas absorption (other than O_3) can be adequately corrected by subtracting ~ 1.20, 0.36, and 0.30 DC from $\langle N_r(\lambda)F_0(\lambda)\rangle_{S_i}$ for Bands 6, 7, and 8, respectively.

4.B. Influence on $L_a + L_{ra}$

For the aerosol component ($L_a + L_{ra}$), we can obtain an upper limit to the gas absorption effect by assuming that the aerosol is confined in a layer near the surface and that the absorption is manifest in the two-way gas transmittance along the propagation path, i.e.,

$$L_a + L_{ra} \longrightarrow (L_a + L_{ra})T_g(\lambda, M),$$

where $T_g(\lambda, M)$ is the two-way transmittance of the atmosphere in the absence of Rayleigh scattering, aerosol scattering, and Ozone absorption. M is the two-way air mass. Equivalently, from Section 3B,

$$\langle \varepsilon(\lambda, \lambda_0)\rangle_{F_0S_i} \longrightarrow \langle T_g(\lambda, M)\varepsilon(\lambda, \lambda_0)\rangle_{F_0S_i} \approx \langle T_g(\lambda, M)\exp[c(\lambda_0 - \lambda)]\rangle_{F_0S_i}.$$

Table 9 compares $\langle \varepsilon(\lambda, 865)\rangle_{F_0S_i}$ with gas absorption with $\varepsilon(\lambda_i, 865)$ for $c = 0$ and 2×10^{-3} nm^{-1} in the LOWTRAN Tropical atmosphere with $M = 3$. Comparison with Table 4 (similar to

Table 9: Comparison between $\langle \varepsilon(\lambda, 865)\rangle_{F_0S_i}$ with gas absorption and $\varepsilon(\lambda_i, 865)$ for the LOWTRAN Tropical atmosphere with $M = 3$.

Band	c (nm^{-1})			
i	0		2×10^{-3}	
	$\langle \varepsilon(\lambda, 865)\rangle_{F_0S_i}$	$\varepsilon(\lambda_i, 865)$	$\langle \varepsilon(\lambda, 865)\rangle_{F_0S_i}$	$\varepsilon(\lambda_i, 865)$
1	1.0000	1.0000	2.4645	2.4744
2	1.0000	1.0000	2.3192	2.3257
3	0.9997	1.0000	2.1109	2.1170
4	0.9999	1.0000	2.0349	2.0340
5	0.9972	1.0000	1.8549	1.8589
6	0.9842	1.0000	1.4608	1.4770
7	0.9802	1.0000	1.1973	1.2214
8	0.9606	1.0000	0.9728	1.0000

Table 9 but without gas absorption and, therefore, independent of M) shows that the addition of gas absorption changes the character of $\langle \varepsilon(\lambda, 865)\rangle_{F_0S_i}$ in the red and the NIR, i.e., instead of

$\langle \varepsilon(\lambda, 865) \rangle_{F_0 S_i}$ being $\sim 1.3\%$ greater than unity for $c = 2 \times 10^{-3}$ nm^{-1}, gas absorption causes it to become $\sim 3\%$ less than unity. Such a variation will have a significant impact on atmospheric correction.

4.C . Influence on L_w

The assessment of gas absorption on $t(\lambda)L_w(\lambda)$ is particularly simple in the case of SeaWiFS. For Bands 1–5 there is essentially no effect, since they have small response for $\lambda \gtrsim 600$ nm, and for Bands 6–8 the effects is also negligible since most of their strong out-of-band response (and the source of most of their out-of-band radiance) is in regions of little gas absorption. Thus, gas absorption can be ignored for this term.

5. Atmospheric Correction

To effect atmospheric correction, i.e., to extract $\langle tL_w(\lambda) \rangle_{S_i}$, we need to compute

$$\langle tL_w(\lambda) \rangle_{S_i} = \langle L_t(\lambda) \rangle_{S_i} - \langle L_r(\lambda) \rangle_{S_i} - \langle L_a(\lambda) + L_{ra}(\lambda) \rangle_{S_i}.$$

We have already described the computation of $\langle L_r(\lambda) \rangle_{S_i}$, and $\langle L_t(\lambda) \rangle_{S_i}$ is the measured radiance, so the problem is to estimate $\langle L_a(\lambda) + L_{ra}(\lambda) \rangle_{S_i}$. We first examine estimation of this quantity in the approximation that $C\left(\theta_v, \phi_v, \theta_0, \phi_0, L_a^{ss}(\lambda), \lambda\right)$ is independent of $L_a^{ss}(\lambda)$ and λ. This is in essence the single scattering approximation, and much of the analysis can be carried out analytically. It will enable a quantitative estimate of the seriousness of the out-of-band response perturbation on atmospheric correction. Then we follow with a technique for including the out-of-band effects in the full multiple scattering algorithm.

5.A. $C\left(\theta_v, \phi_v, \theta_0, \phi_0, L_a^{ss}(\lambda), \lambda\right)$ independent of $L_a^{ss}(\lambda)$ and λ

Utilizing Eq. (7), and referring to Section 3B on the band-averaged $L_a(\lambda) + L_{ra}(\lambda)$, we see that in this approximation,

$$\langle L_a(\lambda) + L_{ra}(\lambda) \rangle_{S_i} = \frac{\langle F_0(\lambda) \rangle_{S_i}}{\langle F_0(\lambda) \rangle_{S_8}} \varepsilon(i, 8) \langle L_a(\lambda) + L_{ra}(\lambda) \rangle_{S_8},$$

where $\varepsilon(i,8)$ is given by

$$\varepsilon(i,8) \equiv \frac{\langle \varepsilon(\lambda,865)\rangle_{F_0 S_i}}{\langle \varepsilon(\lambda,865)\rangle_{F_0 S_8}}.$$

For the open ocean, $\langle tL_w(\lambda)\rangle_{S_i} \approx 0$, for $i = 7$ and 8 (Table 5), so $\varepsilon(7,8)$ and $\varepsilon(8,8)$ can be estimated at each pixel. The key to the correction algorithm is to be able to extrapolate $\varepsilon(7,8)$ to $\varepsilon(i,8)$. A logical way of addressing this is to assume, by analogy to Eq. (16), that

$$\varepsilon(i,8) = \exp[c'(865 - \lambda_i)], \tag{19}$$

where c' is determined from the SeaWiFS-measured value of $\varepsilon(7,8)$ with $\varepsilon(8,8) = 1$. However, since there is considerable out-of-band contamination in the NIR on $\langle \varepsilon(\lambda,865)\rangle_{F_0 S_8}$, $\varepsilon(i,8)$ will not follow Eq. (19) as well as $\varepsilon(\lambda_i,865)$ follows Eq. (16), and the extrapolation will be inaccurate. Consider the problem of estimating the band-averaged water-leaving radiance in SeaWiFS Band 2 (443 nm) for a case in which $\varepsilon(\lambda_i,865)$ follows Eq. (16) exactly. For the specific examples in Table 9, we can compute both the exact and the extrapolated values of $\varepsilon(i,8)$. These are provided in Table 10. If

Table 10: Comparison between the exact and extrapolated values of $\varepsilon(i,8)$ for the LOWTRAN Tropical atmosphere with $M = 3$.

Band	c (nm^{-1})			
i	0		2×10^{-3}	
	Exact	Extrapolated	Exact	Extrapolated
1	1.041	1.096	2.533	2.562
2	1.041	1.089	2.384	2.402
3	1.041	1.079	2.170	2.179
4	1.041	1.074	2.092	2.090
5	1.038	1.064	1.907	1.904
6	1.025	1.040	1.502	1.500
7	1.020	1.020	1.231	1.231
8	1.000	1.000	1.000	1.000

we used the extrapolated values of $\varepsilon(2,8)$ given in Table 10, the extrapolated values would be in error by ~ 1 and 5% for $c = 2\times10^{-3}$ and $c = 0$ nm^{-1}, respectively. Are these serious errors? Noting that an error in $\langle L_a(\lambda) + L_{ra}(\lambda)\rangle_{S_i}$ will lead to an identical error in $\langle t(\theta_v,\lambda)L_w(\lambda)\rangle_{S_i}$, it is easy to show that an error $\Delta\varepsilon(i,8)$ in $\varepsilon(i,8)$ will result in an error $\Delta\langle t(\theta_v,\lambda)L_w(\lambda)\rangle_{S_i}$ in $\langle t(\theta_v,\lambda)L_w(\lambda)\rangle_{S_i}$ given by

$$\frac{\Delta\varepsilon(i,8)}{\varepsilon(i,8)} = \frac{\Delta\langle t(\theta_v,\lambda)L_w(\lambda)\rangle_{S_i}}{\langle L_a(\lambda) + L_{ra}(\lambda)\rangle_{S_i}} = \frac{\langle t(\theta_v,\lambda)\Delta L_w(\lambda)\rangle_{S_i}}{\langle L_w(\lambda)\rangle_{S_i}} \frac{\langle L_w(\lambda)\rangle_{S_i}}{\langle L_a(\lambda) + L_{ra}(\lambda)\rangle_{S_i}}.$$

To achieve a desired fractional error in $\langle L_w(\lambda)\rangle_{S_i} \leq p$,

$$\frac{\Delta\varepsilon(i,8)}{\varepsilon(i,8)} \leq t(\theta_v,i)\frac{\langle L_w(\lambda)\rangle_{S_i}}{\langle L_a(\lambda)+L_{ra}(\lambda)\rangle_{S_i}}\,p,$$

where $t(\theta_v,i)$ is given by Eq. (18). We can estimate the effect of $\Delta\varepsilon(i,8)$ by using the simulations presented in Ref. 2, in which the reflectance ρ, defined to be $\pi L/F_0\cos\theta_0$, was used in place of the

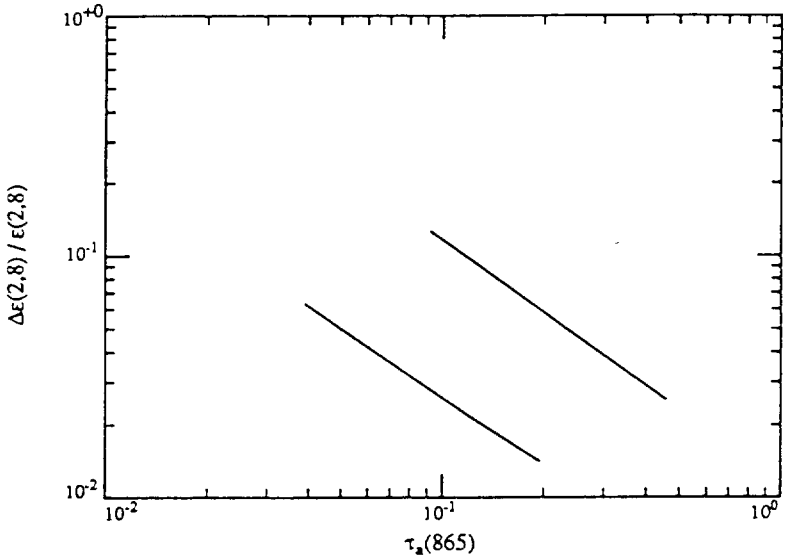

Figure 5. Maximum value of $\Delta\varepsilon(2,8)/\varepsilon(2,8)$ as a function of τ_a required to provide maintain an error in the water-leaving radiance in Band 2 of less than 5% as described in the text. The lower curve is for the T70 aerosol model and the upper curve for M98.

radiance. We note that

$$\langle\rho(\lambda)\rangle_{F_0S_i} = \frac{\pi\langle L(\lambda)\rangle_{S_i}}{\langle F_0(\lambda)\rangle_{S_i}\cos\theta_0},$$

so

$$\frac{\Delta\varepsilon(i,8)}{\varepsilon(i,8)} \leq t(\theta_v,i)\frac{\langle\rho_w(\lambda)\rangle_{F_0S_i}}{\langle\rho_a(\lambda)+\rho_{ra}(\lambda)\rangle_{F_0S_i}}\,p = t(\theta_v,i)t(\theta_0,i)\frac{\langle[\rho_w(\lambda)]_N\rangle_{F_0S_i}}{\langle\rho_a(\lambda)+\rho_{ra}(\lambda)\rangle_{F_0S_i}}\,p.$$

Now, for clear water, e.g., the Sargasso Sea in summer, $\langle[\rho_w(\lambda)]_N\rangle_{F_0S_2} \approx 0.038$, and for the simulations in Ref. 2, $\theta_0 = 60°$ and $\theta_v = 45°$, so $M = 3.41$. Eq. (2) gives $t(\theta_v,2)t(\theta_0,2) \approx 0.66$. Then, for a 5% error ($p = 0.05$) in Band 2,

$$\frac{\Delta\varepsilon(2,8)}{\varepsilon(2,8)} \leq \frac{0.00125}{\langle\rho_a(\lambda)+\rho_{ra}(\lambda)\rangle_{S_2}}.$$

Gordon and Wang's[2] Figure 2 can be used to provide $\langle \rho_a(\lambda) + \rho_{ra}(\lambda) \rangle_{S_2}$, since band averaging of this has little effect in the short-wave bands. This quantity can be related to the aerosol optical thickness, $\tau_a(\lambda)$, at 865 nm. [Note, one also needs to know that $\tau_a(443)/\tau_a(865) = 1.089$ and 2.558 for the M98 and T70 models, respectively.] The result of this exercise is presented in Figure 5. For a given $\tau_a(865)$, the required $\Delta\varepsilon(2,8)/\varepsilon(2,8)$ must be four times smaller for the T70 model compared to the M98, the two extreme models in Ref. 2. The T70 model has $c \approx 1.8 \times 10^{-3}$ nm^{-1}, so $\Delta\varepsilon(2,8)/\varepsilon(2,8) \approx +0.01$ (Table 10) and retrieving $\langle L_w(\lambda) \rangle_{S_2}$ with an error $< 5\%$ would be impossible for $\tau_a(865) \gtrsim 0.3$ (Figure 5). In contrast, the M98 model has $c \approx 0$ so $\Delta\varepsilon(2,8)/\varepsilon(2,8) \approx +0.05$, and insuring a $< 5\%$ error in $\langle L_w(\lambda) \rangle_{S_2}$ would require $\tau_a(865) \lesssim 0.2$.

It is possible to overcome these limitations on the aerosol optical thickness by recognizing that the error in the extrapolated value of $\varepsilon(2,8)$ is entirely due to the difference between $\varepsilon(\lambda_i, 865)$ and $\langle \varepsilon(\lambda, 865) \rangle_{F_0 S_i}$ for $i = 7$ and 8 (Table 9), i.e., the out-of-band response in Bands 7 and 8. That is, if we know the approximate value of c, e.g., c', it should be possible to assess the out-of-band influence on $\varepsilon(7,8)$, the basis for the extrapolation procedure. Unfortunately, the error in extrapolation shows a significant dependence on the water vapor content of the atmosphere. This is demonstrated in Table 11 which provides the error $\Delta\varepsilon(2,8)/\varepsilon(2,8)$ for $c = 0$, $M = 3$ and the six LOWTRAN atmospheric models. Since the water vapor concentration will generally be

Table 11: Error (%) in the extrapolated value of $\varepsilon(2,8)$ for $c = 0$ and $M = 3$ as a function of the water vapor concentration (w) in the LOWTRAN atmospheric models.

LOWTRAN model	w g/cm^2	$\Delta\varepsilon(2,8)/\varepsilon(2,8)$
Tropical	3.332	4.60
Midlatitude summer	2.356	3.83
Midlatitude winter	0.686	2.02
Subarctic summer	1.653	3.16
Subarctic winter	0.328	1.43
U.S. Standard	1.125	2.59

unknown, we also need to understand the influence of choosing an incorrect concentration on which to improve the extrapolation.

It is relatively simple to define a procedure for improving the extrapolation of $\varepsilon(7,8)$ to $\varepsilon(i,8)$. Let

$$f_i(c,M,w) \equiv \frac{\langle \varepsilon(\lambda,865)\rangle_{F_0 S_i}}{\varepsilon(\lambda_i,865)},$$

where w is the total columnar water vapor concentration, and for a given viewing geometry and model, c is defined by Eq. (16). Then, $\varepsilon(i,8)$ is given by

$$\varepsilon(i,8) = \frac{f_i(c,M,w)}{f_8(c,M,w)}\varepsilon(\lambda_i,865). \tag{20}$$

Assuming that the functions $f_i(c,M,w)$ are known, $\varepsilon(i,8)$ can be estimated in the following manner: (1) the initial value of $\varepsilon(7,8)$, i.e., uncorrected for out-of-band effects on $\langle L_a + L_{ra}\rangle_{F_0 S_i}$, is used in Eq. (19) to estimate c'; (2) this value of c' is used in the place of c to estimate $f_i(c,M,w)$; (3) $f_i(c',M,w)$ and the initial value of $\varepsilon(7,8)$ are used in Eq. (20) to estimate $\varepsilon(\lambda_7,865)$, which in turn is used in Eq. (16) to provide a better estimate of c; (4) this estimate of c is used in Eq. (16) to obtain $\varepsilon(\lambda_i,865)$; and (5) Eq. (20) is used to obtain the final estimate of $\varepsilon(i,8)$. After step (4), new values of $f_i(c,M,w)$ could be deduced using the improved estimate of c, if necessary.

To operate this procedure, we need the functions $f_i(c,M,w)$. Through multiple least-squares analysis, we have found that they can be reasonably well represented by the equation

$$\begin{aligned} f_i(c,M,w) = {} & (a_{01} + a_{02}M) + (a_{03} + a_{04}M)c \\ & + \left[(a_{11} + a_{12}M) + (a_{13} + a_{14}M)c\right]w \\ & + \left[(a_{21} + a_{22}M) + (a_{23} + a_{24}M)c\right]w^2, \end{aligned} \tag{21}$$

where the coefficients a_{nm} for SeaWiFS Bands 6, 7, and 8, are provided in Table 12. Figure 6 compares the fitted and the true values of $f_i(c,M,w)$ for SeaWiFS Band 8, and suggests that given M and the aerosol model (c), $f_8(c,M,w)$ can be estimated with an error of $\lesssim 0.1-0.2\%$. The fits to Eq. (21) for SeaWiFS Bands 6 and 7 are much better than that in Figure 6, and for SeaWiFS Bands 1–5 we can assume $f_i(c,M,w) = 1$ (Table 9).

We have examined the efficacy of this procedure by considering the case $M = 3$, and a LOWTRAN Tropical atmosphere. First we assumed that the water vapor concentration is known ($w = 3.322$ g/cm^2), and then examined the effect of an error in w. Thus, initially only the value of c was unknown. The above procedure provided $\varepsilon(2,8) = 1.045$ compared to the correct value of 1.041, a +0.4% error. If the water vapor concentration were also unknown, the error would be

larger. For a concentration 1.318 g/cm^2 (midway between the lowest and highest LOWTRAN concentrations) the procedure yielded $\varepsilon(2,8) = 1.063$ or an error of $\sim +2\%$. Note that even without an accurate value of w, the procedure reduced the error in $\varepsilon(2,8)$ by more than a factor of 2,

Table 12: Coefficients a_{nm} in Eq. (21) for SeaWiFS bands 6, 7, and 8, for c in nm^{-1} and w in gm/cm^2. Notation ± 2 stands for $10^{\pm 2}$, etc.

Coefficient	a_{nm}		
	Band 6	Band 7	Band 8
a_{01}	+9.986 −1	+9.983 −1	+9.958 −1
a_{02}	−7.046 −4	−8.214 −4	−1.561 −3
a_{03}	+2.459 +0	−4.094 −1	+6.442 +0
a_{04}	+2.545 −3	+3.732 −2	−1.894 −2
a_{11}	−1.644 −3	−3.537 −3	−6.337 −3
a_{12}	−1.188 −3	−1.303 −3	−2.679 −3
a_{13}	−1.015 −2	+1.767 −1	−1.037 −2
a_{14}	−8.021 −3	+8.578 −3	−3.583 −2
a_{21}	+1.378 −4	+3.686 −4	+6.157 −4
a_{22}	+1.079 −4	+1.534 −4	+3.080 −4
a_{23}	+1.233 −3	−2.471 −2	−2.428 −3
a_{24}	+4.105 −4	−2.145 −3	+3.628 −3

i.e., from 1.096 to 1.063 compared to the correct 1.041. This would extend the $\tau_a(865)$ limit for a 5% error in $\langle [\rho_w(\lambda)]_N \rangle_{F_0 S_2}$ from ~ 0.3 to ~ 0.5 (Figure 4). However, it is clear that because of the significant out-of-band responses of SeaWiFS Bands 7 and 8, the variation of the water vapor content of the atmosphere limits the accuracy of atmospheric correction at larger values of $\tau_a(865)$.

The procedure outlined in this section can be directly incorporated into the simple correction algorithm described by Wang and Gordon[12] that ignored multiple scattering.

5.B. Inclusion of multiple scattering

Switching from radiance (L) to reflectance (ρ), in the presence of multiple scattering $\rho_a^{\prime\prime}(\lambda)$ is replaced by

$$\rho_a(\lambda) + \rho_{ra}(\lambda) = C\left(\theta_v, \phi_v, \theta_0, \phi_0, \rho_a^{\prime\prime}(\lambda), \lambda\right) \rho_a^{\prime\prime}(\lambda) \tag{22}$$

where C is a weak function of $\rho_a^{ss}(\lambda)$ and λ. In the band-averaged case, we must deal with $\langle \rho_a(\lambda) + \rho_{ra}(\lambda) \rangle_{F_0 S_i}$. Because of the weak dependence of C on $\rho_a^{ss}(\lambda)$ and λ, we can ignore the out-of-band effects on C and approximate $\langle \rho_a(\lambda) + \rho_{ra}(\lambda) \rangle_{F_0 S_i}$ by

$$\begin{aligned} \langle \rho_a(\lambda) + \rho_{ra}(\lambda) \rangle_{F_0 S_i} &= C\Big(\theta_v, \phi_v, \theta_0, \phi_0, \rho_a^{ss}(\lambda_i), \lambda_i\Big) \langle \rho_a^{ss}(\lambda) \rangle_{F_0 S_i} \\ &= C\Big(\theta_v, \phi_v, \theta_0, \phi_0, \rho_a^{ss}(\lambda_i), \lambda_i\Big) \left[\frac{\langle \varepsilon(\lambda, 865) \rangle_{F_0 S_i}}{\varepsilon(\lambda_i, 865)} \rho_a^{ss}(\lambda_i) \right], \\ &= C\Big(\theta_v, \phi_v, \theta_0, \phi_0, \rho_a^{ss}(\lambda_i), \lambda_i\Big) f_i(c, M, w) \rho_a^{ss}(\lambda_i), \end{aligned} \tag{23}$$

i.e., in the band-averaged case $\rho_a^{ss}(\lambda)$ outside of the argument of C in Eq. (22) is replaced by $f_i(c, M, w)\rho_a^{ss}(\lambda_i)$, in Eq. (23). Since the influence of multiple scattering on the algorithm is

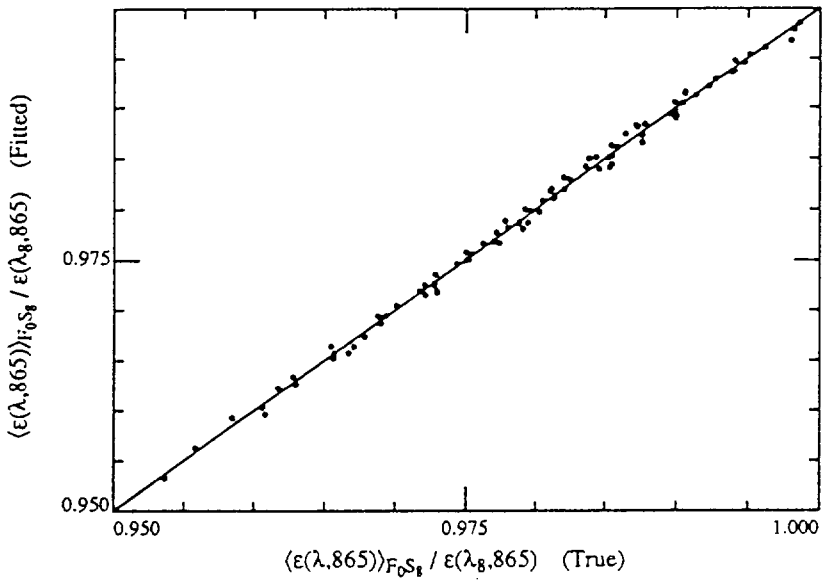

Figure 6. Comparison between the true values of $\langle \varepsilon(\lambda, 865) \rangle_{F_0 S_8} / \varepsilon(\lambda_8, 865)$ with those computed using Eq. (21) and Table 12.

contained in the dependence of C on $\rho_a^{ss}(\lambda)$ and λ, retaining the dependence of C on $\rho_a^{ss}(\lambda_i)$ and λ_i in Eq. (23) will retain the multiple scattering effects in the algorithm. For a given aerosol model (known c), $f_i(c, M, w)$ can be estimated given the water vapor content and the viewing geometry using Eq. (21). In the Gordon and Wang[2] multiple scattering algorithm, $\rho_a(\lambda_i) + \rho_{ra}(\lambda_i)$ determined from $\rho_t(\lambda_i) - \rho_r(\lambda_i)$ for $i = 7$ and 8 is used in Eq. (22) to estimate $\rho_a^{ss}(\lambda_i)$, which in turn is used to estimate $\rho_a(\lambda_i) + \rho_{ra}(\lambda_i)$ for $i = 1$ to 6. When the out-of-band response is included, $\langle \rho_a(\lambda) + \rho_{ra}(\lambda) \rangle_{F_0 S_i}$ for $i = 7$ and 8 is used in Eq. (23) to estimate $\rho_a^{ss}(\lambda_i)$, which is used

in a similar manner to estimate $\langle \rho_a(\lambda) + \rho_{ra}(\lambda) \rangle_{F_0 S_i}$ for $i = 1$ to 6. This approach for including the out-of-band effects is satisfying because the implementation strategy for utilizing Eq. (22) — lookup tables relating $\rho_a(\lambda_i) + \rho_{ra}(\lambda_i)$ to $\rho_a^{ss}(\lambda_i)$ for all sun-viewing geometries and nominal band centers i based on solutions to the radiative transfer equation — can be applied to Eq. (23) using the *same* lookup tables. One need only recognize that when $\langle \rho_a(\lambda) + \rho_{ra}(\lambda) \rangle_{F_0 S_i}$ is entered on the left-hand-side of Eq. (23), the result is $f_i(c, M, w)\rho_a^{ss}(\lambda_i)$ rather than just $\rho_a^{ss}(\lambda_i)$. We envisage implementation of this out-of-band response modification to the multiple scattering atmospheric correction algorithm will be based on a lookup table relating the parameter c in Eq. (16) to the sun-viewing geometry for each model.

6. Concluding remarks

A methodology for delineating the influence of finite spectral band widths and significant out-of-band response on ocean color imagery was described and applied to SeaWiFS. The basis of the method is the application of the sensor's spectral response functions to the individual components of the TOA radiance. The importance of the examination of the individual components is that it provides an avenue for estimating the impact on the entire ocean color system — sensor plus algorithms.

As might be expected, the most significant effects of finite band widths and out-of-band response occurs for components with a very strong spectral variation, e.g., $L_r(\lambda)$ and $L_w(\lambda)$. In the case of SeaWiFS Band 8 (865 nm), it is shown that the significant out-of-band response in the blue requires that an optical thickness of 0.0169 $[\langle \tau_r(\lambda) \rangle_{F_0 S_8}]$ rather than 0.0155 $[\tau_r(865)]$ be used to predict $\langle L_r(\lambda) \rangle_{S_8}$. In fact, as much as 9% of $\langle L_r(\lambda) \rangle_{S_8}$ is due to $L_r(\lambda)$ for $\lambda < 600$ nm. For the water-leaving radiance, the error in replacing $\langle L_w(\lambda) \rangle_{S_i}$ by its narrow-band counterpart, $L_w(\lambda_i)$, is of the order of a few percent in the blue-green bands. This implies that verification that the SeaWiFS system — sensor plus algorithms — meets the goal of providing the water-leaving radiance in the blue in clear ocean water to within 5% will require measurements of $L_w(\lambda)$ through out the visible rather than just in a narrow (10–20 nm) spectral band around λ_2. In the NIR, a large fraction (Table 5) of $\langle L_w(\lambda) \rangle_{S_i}$ is the result of the out-of-band response of the sensor; however, $\langle L_w(\lambda) \rangle_{S_i}$ is still usually $\lesssim 1$ DC, so these bands can still be used for atmospheric correction.

Gaseous absorption (other than Ozone) is mostly confined to the red and NIR spectral regions (Figures 3 and 4). Thus, we expect its influence to be strongest for $\lambda \gtrsim 600$ nm, and strongest for the components of $L_t(\lambda)$ that have a weak spectral dependence. In fact, there is little or no influence of gaseous absorption on $\langle L_w(\lambda)\rangle_{S_i}$, and for $\langle L_r(\lambda)\rangle_{S_i}$ the influence is only ≈ 1 DC for Band 6 and < 1 DC for Bands 7 and 8. In contrast, gaseous absorption is important for the aerosol component. It can cause a significant reduction (a few percent) in the aerosol component in Bands 6, 7, and 8.

By assuming that the aerosols reside in a thin layer near the surface (the marine boundary layer), it is found that atmospheric correction of SeaWiFS can be degraded by the influence of water vapor absorption in the shoulders of Bands 7 and 8. This causes an apparent spectral variation of $L_a + L_{ra}$ between these two bands that would be uncharacteristic of the aerosol present, leading to an error in atmospheric correction. This effect is dependent on the water vapor content of the atmosphere. At typical water vapor concentrations, the error is larger for aerosols with weak spectral variation in reflectance than for those displaying a strong spectral variation. If the content is known, a simple procedure can be used to reduce the degradation of the atmospheric correction in both single- and multiple-scattering approaches. Uncertainty in the water vapor content will limit the accuracy of the SeaWiFS correction algorithm.

Appendix

The nominal radiometric characteristics of SeaWiFS[1] are presented in Table 13. In the table, λ represents the spectral pass band of each of the instrument's spectral bands. The detailed spectral response functions that were used in the text for each band are presented in Barnes et al.[7] L_{Sat} is the saturation radiance at the lower ocean-viewing sensitivity. There are three other radiometric sensitivities: two for stability monitoring by viewing sun light reflected from an internal diffuser

Table 13: Nominal SeaWiFS instrument parameters.

Band	λ nm	L_{Sat} mW/cm^2 μm Sr
1	402–422	13.63
2	433–453	13.25
3	480–500	10.50
4	500–520	9.08
5	545–565	7.44
6	660–680	4.20
7	745–785	3.00
8	845–885	2.13

(short-term) or from the moon (long-term); and one for ocean viewing at large solar zenith angles. The saturation radiance for the second (higher) ocean-viewing sensitivity is $\sim L_{Sat}/2$, i.e., it has twice the radiometric sensitivity of the lower. The radiance data are 10-bit digitized on-board the space craft, so 1 digital count (DC) of radiance is approximately $L_{Sat}/1024$. When DC's are mentioned in the text, unless otherwise noted, the reference is to those corresponding to the *lower* ocean-viewing sensitivity (Table 13). Signal-to-noise ratios are generally of the order of 500 for input radiances at $\sim \frac{1}{2}$ to $\frac{3}{4}$ of L_{Sat}, so the sensor noise will be of the order of 1 DC for all bands.

References

[1] S. B. Hooker, W. E. Esaias, G. C. Feldman, W. W. Gregg and C. R. McClain, *SeaWiFS Technical Report Series: Volume 1, An Overview of SeaWiFS and Ocean Color* (NASA, Greenbelt, MD, Technical Memorandum 104566, July 1992).

[2] H. R. Gordon and M. Wang, "Retrieval of water-leaving radiance and aerosol optical thickness over the oceans with SeaWiFS: A preliminary algorithm," Applied Optics **33**, 443–452 (1994).

[3] P. Y. Deschamps, M. Herman and D. Tanre, "Modeling of the atmospheric effects and its application to the remote sensing of ocean color," Applied Optics **22**, 3751–3758 (1983).

[4] H. R. Gordon, D. K. Clark, J. L. Mueller and W. A. Hovis, "Phytoplankton pigments derived from the Nimbus–7 CZCS: initial comparisons with surface measurements," Science **210**, 63–66 (1980).

[5] H. R. Gordon, D. K. Clark, J. W. Brown, O. B. Brown, R. H. Evans and W. W. Broenkow, "Phytoplankton pigment concentrations in the Middle Atlantic Bight: comparison between ship determinations and Coastal Zone Color Scanner estimates," Applied Optics **22**, 20–36 (1983).

[6] H. R. Gordon, J. W. Brown and R. H. Evans, "Exact Rayleigh Scattering Calculations for use with the Nimbus-7 Coastal Zone Color Scanner," Applied Optics **27**, 862–871 (1988).

[7] R. A. Barnes, A. W. Holmes, W. L. Barnes, W. E. Esaias, C. R. McClain and T. Svitek, *SeaWiFS Technical Report Series: Volume 23, SeaWiFS Prelaunch Radiometric Calibration and Spectral Characterization* (NASA, Greenbelt, MD, Technical Memorandum 104566, October 1994).

[8] J. E. Hansen and L. D. Travis, "Light Scattering in Planetary Atmospheres," Space Science Reviews **16**, 527–610 (1974).

[9] J. -M. André and A. Morel, "Simulated Effects of Barometric Pressure and Ozone Content Upon the Estimate of Marine Phytoplankton From Space," Jour. Geophys. Res. **94C**, 1029–1037 (1989).

[10] M. Nicolet, "The solar spectral irradiance and its action in the atmospheric photodissociation processes," Planet. Space Sci. **29**, 951–974 (1981).

[11] H. Neckel and D. Labs, "The Solar Radiation Between 3300 and 12500 Å," Solar Physics **90**, 205–258 (1984).

[12] M. Wang and H. R. Gordon, "A Simple, Moderately Accurate, Atmospheric Correction Algorithm for SeaWiFS," *Remote Sensing of Environment* **50**, 321–239 (1994).

[13] E. P. Shettle and R. W. Fenn, *Models for the Aerosols of the Lower Atmosphere and the Effects of Humidity Variations on Their Optical Properties* (Air Force Geophysics Laboratory, Hanscomb AFB, MA 01731, AFGL–TR–79-0214, 1979).

[14] F. X. Kenizys, E. P. Shettle, W. O. Gallery, J.H.Chetwynd, L. W. Abreu, J. E. A. Selby, S. A. Clough and R. W. Fenn, *Atmospheric Transmittance/Radiance: The LOWTRAN 6 Model* (Air Force Geophysics Laboratory, Hanscomb AFB, MA 01731, AFGL–TR–83–0187, 1983) NTIS AD A137796.

[15] H. R. Gordon, O. B. Brown, R. H. Evans, J. W. Brown, R. C. Smith, K. S. Baker and D. K. Clark, "A Semi-Analytic Radiance Model of Ocean Color," Jour. Geophys. Res. **93D**, 10909–10924 (1988).

[16] H. R. Gordon and D. K. Clark, "Clear water radiances for atmospheric correction of coastal zone color scanner imagery," Applied Optics **20**, 4175–4180 (1981).

[17] D. K. Clark, "Phytoplankton Algorithms for the Nimbus-7 CZCS," in *Oceanography from Space*, edited by J. R. F. Gower (Plenum Press, New York, NY, 1981) p. 227–238.

[18] H. R. Gordon and K. Ding, "Self-Shading of In-Water Optical Instruments," Limnology and Oceanography **37**, 491–500 (1992).

[19] F. X. Kneizys, E. P. Shettle, L. W. Abreu, J. H. Chetwynd, G. P. Anderson, W. O. Gallery, J. E. A. Selby and S. A. Clough, *Users Guide to LOWTRAN 7* (Air Force Geophysics Laboratory, AFGL-TR-88-0177, 1988).

[20] K. Ding and H. R. Gordon, "Analysis of the influence of O_2 *A* band absorption on atmospheric correction of ocean color imagery," Applied Optics **34**, 2068–2080 (1995).